Structural phase transitions of Si(111)-($\sqrt{3}\times\sqrt{3}$)$R30°$-Au: Phase transitions in domain-wall configurations

T. Nagao* and S. Hasegawa
Department of Physics, Graduate School of Science, University of Tokyo, 7-3-1 Hongo, Bunkyo-Ku, Tokyo 113, Japan and Core Research and Evolutional Science and Technology, Japan Science and Technology Corporation, Kawaguchi Center Building, 1-8 Honcho 4-chome, Kawaguchi-city, Saitama 332, Japan

K. Tsuchie and S. Ino†
Department of Physics, Graduate School of Science, University of Tokyo, 7-3-1 Hongo, Bunkyo-Ku, Tokyo 113, Japan

C. Voges, G. Klos, H. Pfnür, and M. Henzler
Institut für Festkoeorperphysik, Universität Hannover, Appelstrasse 2, D-30167 Hannover, Germany
(Received 8 April 1997; revised manuscript received 4 November 1997)

Behaviors of domain walls on the Au-adsorbed Si(111)-$\sqrt{3}\times\sqrt{3}$ and 6×6 surfaces have been investigated by spot-profile-analyzing low-energy electron diffraction and scanning tunneling microscopy. A continuous change from the α-$\sqrt{3}\times\sqrt{3}$ pattern to the β-$\sqrt{3}\times\sqrt{3}$ pattern in diffraction at room temperature has been correlated to the increase in domain-wall density and their characteristic configuration change as a function of Au coverage $\Theta=0.76-0.96$. It has been found that the sharp $\sqrt{3}\times\sqrt{3}$ spikes persists irrespective of the domain-wall morphology. The zigzagging domain walls at $\Theta=0.79$ at room temperature are found to transform to roundish ones at 753 K, and finally decompose completely to vanish around 893 K resulting in apparent large domains of $\sqrt{3}\times\sqrt{3}$ structure. Above $\Theta=0.96$, the domain walls are proposed to arrange with a long-range order with 6×6 periodicity when the sample is annealed at around 600 K and slowly cooled. On the contrary, metastable amorphous arrangement in the domain walls with average separation of 6**a** (where **a** is the substrate lattice period) is formed after annealing followed by quench cooling, which corresponds to the β-$\sqrt{3}\times\sqrt{3}$ structure. [S0163-1829(98)08415-X]

I. INTRODUCTION

Structural phase transitions in two-dimensional (2D) systems have attracted wide interest in experimental as well as theoretical researches in the past decade. Gas-adsorbed layers on unreconstructed metal surfaces have been extensively and successfully studied as test systems for order-disorder phase transitions of lattice-gas models.[1–4] In spite of the heavy reconstructions involving substrate atoms, phase transitions of some metal-induced superstructures on semiconductor surfaces have been also understood on the basis of pure symmetry arguments of lattice-gas models.[5–8] For example, an order-disorder phase transition of the Si(111)-($\sqrt{3}\times\sqrt{3}$)$R30°$-Au phase around 1000 K was found to be in good agreement with the three-state Potts model, which was expected from the symmetry considerations.[7]

In addition to the order-disorder phase transitions around 1000 K,[5–8] the Au/Si(111) system exhibits rich diversity of phase transitions characterized by the evolution in fine reflections in electron-diffraction patterns[9,10] (see Fig. 1). Most of these phase transitions are different from the ordinary order-disorder phase transitions in a sense that behaviors of short-range orders govern the peculiar nature of the phase transitions. Origins of these short-range orders were discussed in many preceding works,[11–14] and are now widely accepted that they are arising from partly ordered structural elements as adatoms in 5×2 structure and high-density domain walls in α-$\sqrt{3}\times\sqrt{3}$ structure.[15–21] Since the α-$\sqrt{3}\times\sqrt{3}$ phase links to β-$\sqrt{3}\times\sqrt{3}$ and 6×6 phases by increasing the Au coverage, evolution in the domain-wall configuration is expected to be an essential part of these variegated phase transitions. However, curiously enough, most studies of the $\sqrt{3}\times\sqrt{3}$ and the 6×6 phases were mainly concerned with structure models within the unit cell, and systematic study of the behavior of domain walls have been lacking so far.

In this work, we have studied the structural phase transitions among the α-$\sqrt{3}\times\sqrt{3}$, β-$\sqrt{3}\times\sqrt{3}$, and 6×6 phases both in real space and in reciprocal space by using scanning tunneling microscopy (STM) and spot-profile-analyzing low-energy electron diffraction (SPA-LEED). Unique behaviors in contrast to the conventional order-disorder phase transitions are observed and understood on the basis of characteristic evolution in the domain-wall configurations.

Qualitative descriptions of the domain-wall configurations at each stage of these phase transitions are summarized in Fig. 2. Experimental sequences we will report in Sec. III are shown by the numbers ①–③. In Sec. III A, correlation between the LEED pattern and the domain-wall configuration in the STM image is studied as a function of coverage (sequence ①). In Sec. III B, we report the fluidization and the successive decomposition of the domain walls at elevated temperatures (sequence ②). In Sec. III C, we discuss the structures and the formation mechanisms of β-$\sqrt{3}\times\sqrt{3}$ and the 6×6 structures on the basis of the domain-wall configurations during different cooling procedures (sequence ③).

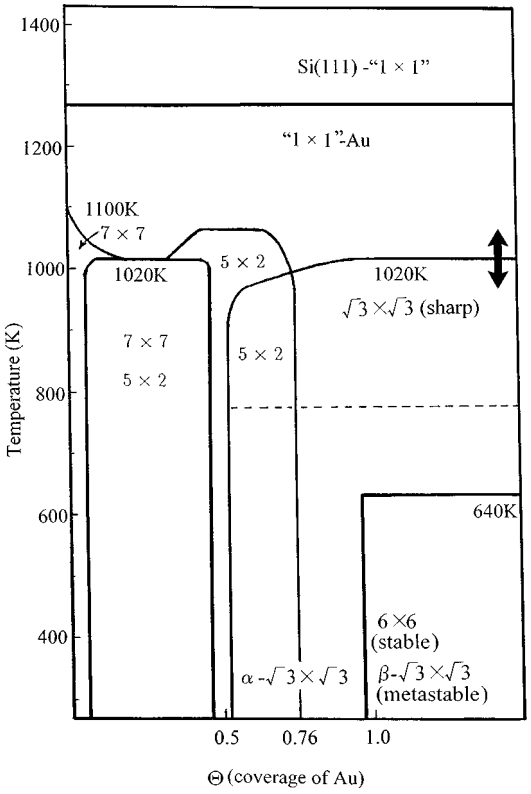

FIG. 1. A phase diagram of the Au-adsorbed Si(111) surface based on the RHEED observation (Ref. 10). Below $\Theta=0.76$ (Θ:Au coverage), 5×2 pattern takes place with 7×7 or α-$\sqrt{3}\times\sqrt{3}$ patterns (pure 5×2 pattern appears in a narrow coverage range around $\Theta=0.5$). Above $\Theta=0.76$, fine reflections in $\sqrt{3}\times\sqrt{3}$ pattern change their feature from α-$\sqrt{3}\times\sqrt{3}$ to β-$\sqrt{3}\times\sqrt{3}$ pattern in a continuous way up to $\Theta=0.96$. At temperatures above 770 K, the fine reflections disappear and only the sharp $\sqrt{3}\times\sqrt{3}$ spots survive. Bold arrows indicate the order-disorder transition reported in Refs. 5–7.

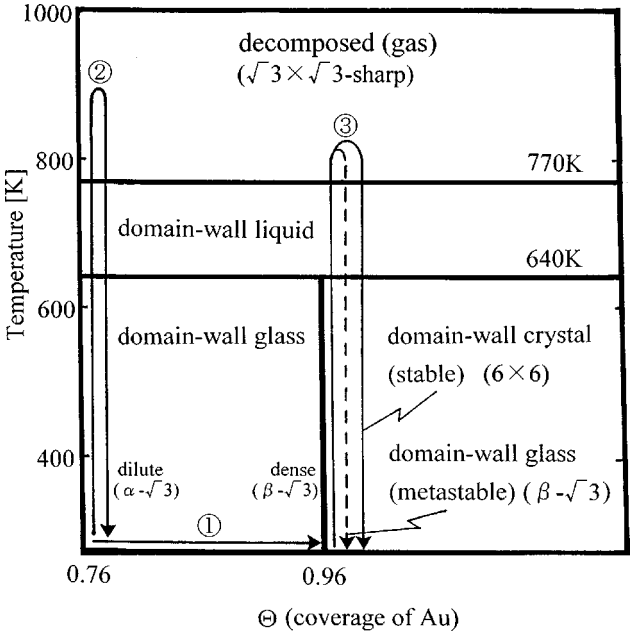

FIG. 2. A schematic phase diagram of the domain walls on Au-adsorbed Si(111) surface above $\Theta=0.76$. Lines denoted by ①, ②, and ③ indicate the three different experimental sequences done in the present study (broken line in ③ corresponds to quench cooling after heating above 800 K). α-$\sqrt{3}$ and β-$\sqrt{3}$ stand for α-$\sqrt{3}\times\sqrt{3}$ and β-$\sqrt{3}\times\sqrt{3}$, respectively.

II. EXPERIMENTAL

Experiments were done in a reflection-high-energy electron-diffraction (RHEED) STM chamber (UNISOKU model USM501; 5×10^{-9} Pa base pressure), and a SPA-LEED chamber (4×10^{-9} Pa base pressure) equipped with a cylindrical mirror analyzer and a quartz thickness monitor. The specimen was cut from highly oriented Si wafers with less than 0.1° misorientation from the (111) face. The surface was cleaned by several flash heatings up to 1450 K with a current fed through the Si wafer, followed by moderate cooling. In the RHEED-STM observations, Au coverage Θ [expressed by the ratio of the Au atom density to the Si atom density in the Si(111) plane] was determined by the duration time in deposition calibrated to the onset of the pure α-$\sqrt{3}\times\sqrt{3}$ pattern that was previously determined to be $\Theta=0.76$ by Rutherford backscattering.[22] The determined coverage for each structure agrees well with other ion-scattering spectroscopic measurements.[23–25] Gold was evaporated from a tungsten basket or an alumina-coated tungsten basket keeping the pressure below 2×10^{-7} Pa. The STM images shown here were taken in topographic (constant current) mode or in current-imaging mode (that is a nearly constant-high mode with slow z-feedback action). In the SPA-LEED experiments, the coverage was determined by a quartz thickness monitor which was also calibrated to the onset of the pure α-$\sqrt{3}\times\sqrt{3}$ pattern. Precision of these coverage determinations was ±0.02.

III. RESULTS AND DISCUSSIONS

A. Continuous phase transition from α-$\sqrt{3}\times\sqrt{3}$ to β-$\sqrt{3}\times\sqrt{3}$: Coverage dependence at RT

At room temperature (RT), the electron-diffraction pattern transforms dramatically from α-$\sqrt{3}\times\sqrt{3}$ to β-$\sqrt{3}\times\sqrt{3}$ in a continuous way within the narrow coverage range of $\Theta=0.76$–0.96.[26] To clarify the correlation between the LEED patterns and the domain-wall configurations, STM images and LEED patterns were taken at RT as a function of Au coverage.

Figure 3(a) shows a wide-scan STM image in current imaging mode taken at a coverage around $\Theta=0.7$ (corresponding to a mixture of 5×2 and α-$\sqrt{3}\times\sqrt{3}$ phases). Meandering features correspond to domain walls of the α-$\sqrt{3}\times\sqrt{3}$ structure, while stripe patterns correspond to the 5×2 domains. The 5×2 region decreases and the α-$\sqrt{3}\times\sqrt{3}$ region increases as the Au coverage increases. Density of the domain walls in the $\sqrt{3}\times\sqrt{3}$ region remains constant up to $\Theta=0.76$, showing that this is the minimum density. At $\Theta=0.76$, the 5×2 region extinguishes and the density of the domain walls starts to increase. Figure 3(b) is an example of the image taken at $+1$ V tip bias in topographic mode at

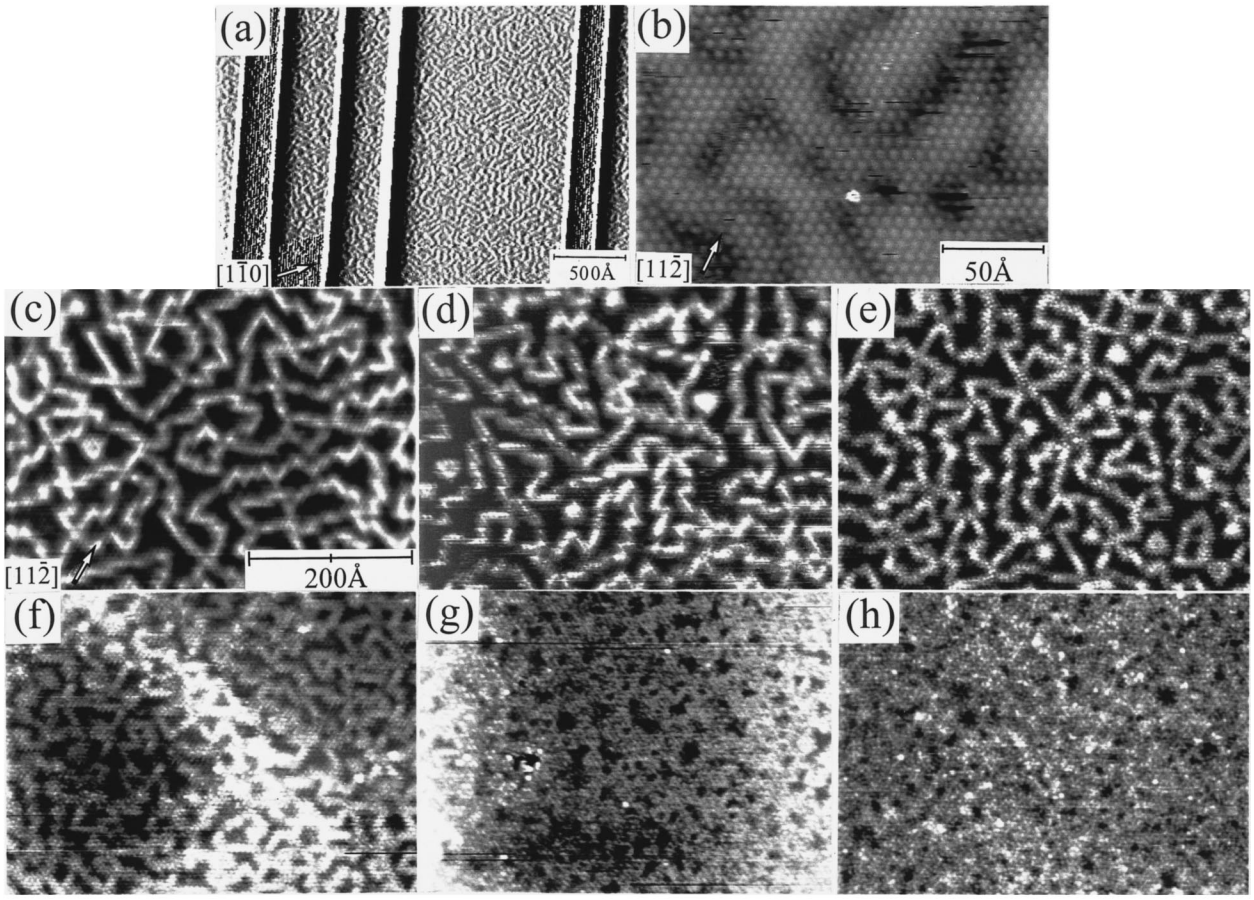

FIG. 3. (a) A STM image taken at a coverage below $\Theta = 0.76$ (a current image). (b) A topographic image at $\Theta = 0.76$ taken with $+1.0$ V tip bias and 0.4 nA tunneling current. (c)–(h) Topographic images taken in a same series of Au deposition at -1.0 V tip bias and 0.4 nA tunneling current. The domain walls appear as distinct bright features, and their density increases continuously. (c) $\Theta = 0.76$ (α-$\sqrt{3} \times \sqrt{3}$), (d) $\Theta = 0.78$ (α-$\sqrt{3} \times \sqrt{3}$), (e) $\Theta = 0.80$, (f) $\Theta = 0.83$, (g) $\Theta = 0.90$, (h) $\Theta = 0.96$ (β-$\sqrt{3} \times \sqrt{3}$).

$\Theta = 0.76$. Commensurate $\sqrt{3} \times \sqrt{3}$ domains are separated by antiphase domain walls which appear as depressed ditches. Feature of the domain walls changes drastically depending on the tip bias: it is normally sharper and distinct at negative tip biases. Figures 3(c)–3(h) show the STM images taken at -1 V tip bias as a function of coverage. As clearly shown in Figs. 3(c)–3(h), the total length of domain wall increases continuously with Au coverage, which shows the domain walls are of (super) heavy type:[18] excess Au atoms are incorporated into the domain walls. A fractional area of the domain walls (bright regions) becomes maximum at $\Theta = 0.96$ [Fig. 3(h)] where the evolution in both the STM image and the diffraction pattern stops even with a further increase of coverage.

Figures 4(a)–4(f) show magnified images in topographic mode taken at the same coverages as Figs. 3(c)–3(h). Some characteristic features of the domain walls are seen in these images. White zigzagging domain walls separate the commensurate antiphase $\sqrt{3} \times \sqrt{3}$ domains. Preferential wall alignment in [112]-type directions can be seen clearly from the STM images as was reported by previous STM work.[18] What is investigated in the present study is the behavior from $\Theta = 0.90$ to $\Theta = 0.96$ [Figs. 3(g), 3(h) and Figs. 4(e), 4(f)], where the diffraction gradually exhibits a character of β-$\sqrt{3} \times \sqrt{3}$ pattern as will be shown below. Since the transition is continuous in electron-diffraction patterns[26] as well as in STM images, it is natural to assume that the domain walls remain also at $\Theta = 0.96$ [Figs. 3(h), 4(f)]. However, to extract some structural features only from the STM images seems hopeless at a glance because of apparent highest complexity.

Electron-diffraction techniques with high resolution serve as efficient tools for extracting general structural features in partially ordered systems like the present case. The patterns taken by SPA-LEED with a transfer width of 2000 Å are shown in Figs. 5(a)–5(d) as a function of Au coverage. Figures 5(a) and 5(b) show a typical feature of α-$\sqrt{3} \times \sqrt{3}$ pattern [satellites around superlattice spots; see the inset in Fig. 5(b)]. Figure 5(d) shows that of the β-$\sqrt{3} \times \sqrt{3}$ pattern (intense rings around fundamental and superlattice spots). Since the transition from α-$\sqrt{3} \times \sqrt{3}$ to β-$\sqrt{3} \times \sqrt{3}$ is continuous, the names of ''α'' and ''β'' are nominal ones that express the characters at the two extremes. Hexagonal feature around the $\sqrt{3} \times \sqrt{3}$ spike [inset in Fig. 5(b)] reflects the average domain size and domain shape. The broad streaks running between sharp spots in Fig. 5(b) correspond to the scattering from domain walls running in [112]-type directions. Ring around (00) spot in the same figure represents the average

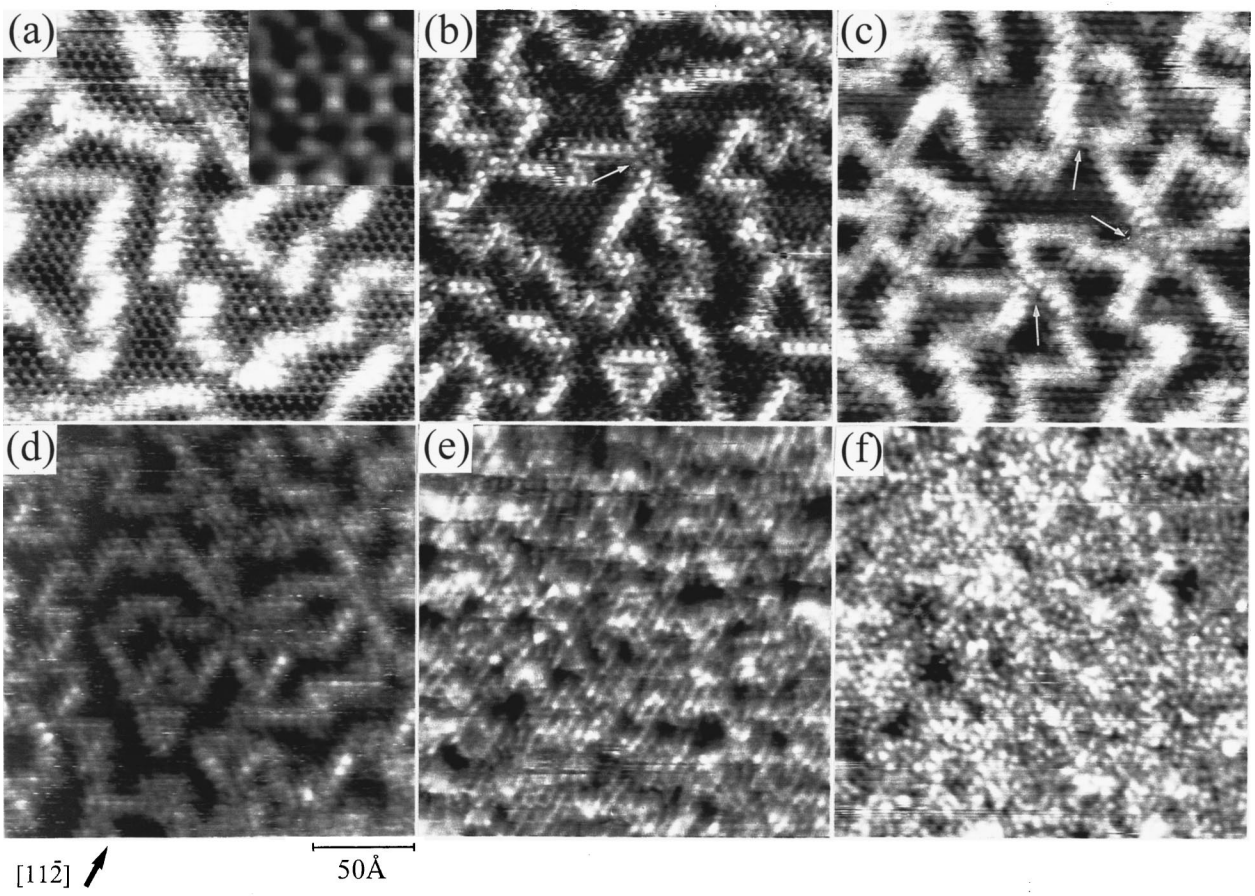

FIG. 4. Magnified topographic images taken in the same series of Au deposition as Fig. 3 (-1.0 V tip bias, 0.4 nA tunneling current). (a) $\Theta=0.76$, (b) $\Theta=0.78$, (c) $\Theta=0.80$, (d) $\Theta=0.83$, (e) $\Theta=0.90$, (f) $\Theta=0.96$. Inset in (a) shows 22 Å$\times$22 Å image of a commensurate $\sqrt{3}\times\sqrt{3}$ region.

separation (about 45 Å) between the domain walls. These fine features convert to diffuser and weaker ones as shown in Fig. 5(c) as the Au coverage increases, since the size of the $\sqrt{3}\times\sqrt{3}$ domains decreases.

In contrast to the intense and sharp $\sqrt{3}\times\sqrt{3}$ spikes, the weak features at around $\Theta=0.90$ [Fig. 5(c)] have been overlooked in many reports. In those works, this pattern was regarded as a ''sharp $\sqrt{3}\times\sqrt{3}$ pattern.'' If a structure determination by averaging technique such as *I-V* measurements in conventional LEED is done at this coverage, where the complexity in domain-wall arrangement is the highest, the meaning of the obtained structure parameters will be obscure. At $\Theta=0.96$ [Fig. 5(d)], the diffuse features convert to distinct rings around (00) and (1/3 1/3) spikes, showing the formation of some short-range order. Formation of the 6×6 pattern [Fig. 5(e)] proceeds in a different way from Figs. 5(a)–5(d) and will be discussed in Sec. III C.

The continuity of the transition from α- to β-$\sqrt{3}\times\sqrt{3}$ can be seen clearly in the spot profile measurements (Fig. 6). It should be noted that features indicated by arrowheads become stronger and sharper at positions where the separations from (00) or (1/3 1/3) spikes are 1/6 of the distance between (00) and (01). These features correspond to the rings in Fig. 5(d). Formation of the rings suggests that domain walls in the β-$\sqrt{3}\times\sqrt{3}$ structure are arranged with an average distances of 6**a**, but not in a 6×6 long-range order (**a** is a primitive translational vector of the substrate 1×1 mesh). The sharp $\sqrt{3}\times\sqrt{3}$ spikes are seen in all these figures [see also Figs. 5(a)–5(d)], which seems quite inconsistent with the STM observation that shows domain-size contraction with coverage increase. This indicates that the sharpness of the spikes has no correlation to the domain size.

For the further discussions concerning the rings in the β-$\sqrt{3}\times\sqrt{3}$ pattern and the existence of the sharp superlattice spikes, we made a simulation. Two-dimensional images imitating some essential features in the STM images, e.g., domain-wall alignment in [112]-type directions and their inflection angles of 60°, are shown together with corresponding Fourier-transformed patterns in Fig. 7. Two types of the domains of three different sublattices are denoted schematically by filled circles on different sites in $\sqrt{3}\times\sqrt{3}$ mesh; one corresponds to the circles on the triangular lattice points, while another corresponds to those at the centers of the triangles. From (a) to (c), the domain-wall density is increased. Streaks and diffuse features around $\sqrt{3}\times\sqrt{3}$ spikes in Fourier-transformed patterns become diffuser as the domain walls become denser, while the fundamental and $\sqrt{3}\times\sqrt{3}$ spikes persist [(d), (e)]. Rings whose radius corresponds to 1/6 of the unit reciprocal vector of Si(111)-1×1 are successfully reproduced when the 2D image is created by distribut-

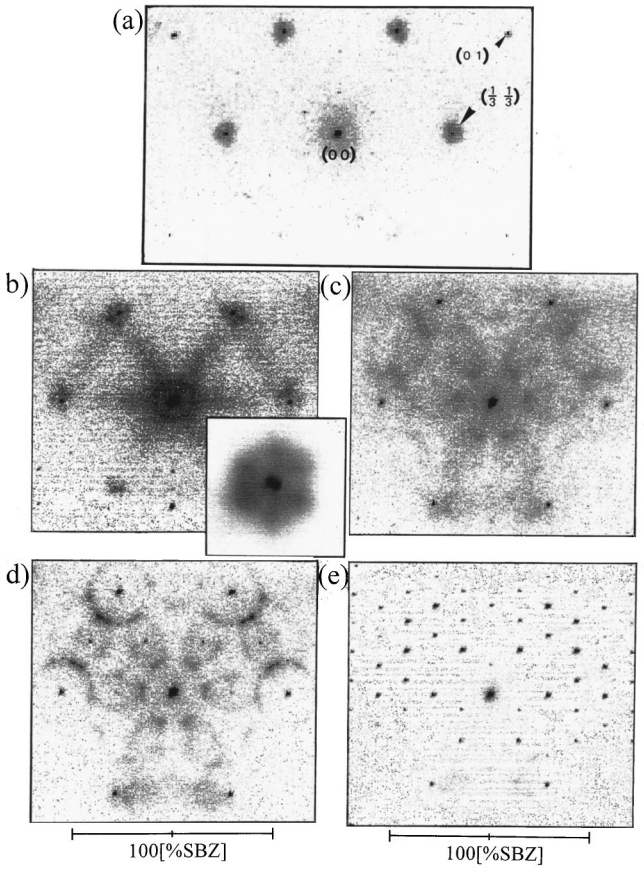

FIG. 5. Evolution of fine structures in the LEED pattern as a function of Au coverage is shown. (a) $\Theta=0.75$ (α-$\sqrt{3}\times\sqrt{3}$), (b) $\Theta=0.79$ (α-$\sqrt{3}\times\sqrt{3}$), (c) $\Theta=0.92$, (d) $\Theta=0.96$ (β-$\sqrt{3}\times\sqrt{3}$), (e) $\Theta=0.96$ (6×6). All data are taken at RT after heating around 850 K. Scales are in the units of a reduced surface Brillouin zone (SBZ) for Si(111)-1×1. Intensities are shown in logarithmic scale.

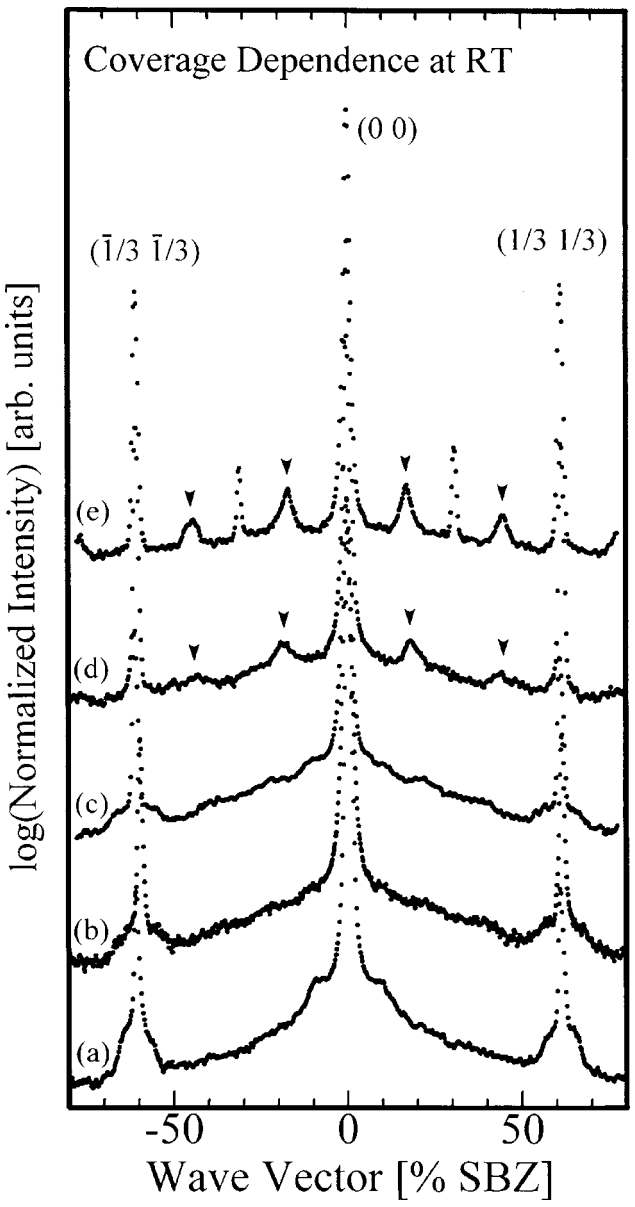

FIG. 6. Evolution of LEED spot profiles in the (00)-(11) direction as a function of Au coverage is shown. (a) $\Theta=0.76$ ($E_p=80.0$ eV), (b) $\Theta=0.79$ ($E=80.0$ eV), (c) $\Theta=0.88$ ($E_p=81.5$ eV), (d) $\Theta=0.93$ ($E=81.6$ eV), (e) $\Theta=1.0$ ($E=81.6$ eV). Arrowheads indicate the features correspond to the rings in Fig. 5(d). All data are taken at RT after heating around 850 K. Scales are in the units of a reduced surface Brillouin zone (SBZ) for Si(111)-1×1. Intensities are normalized to that of (00) spikes and are shown in logarithmic scale.

ing small $\sqrt{3}\times\sqrt{3}$ domains to keep their distances close to 6**a**, but without 6×6 long-range order [see (c) and (f)]. Most of the domains are minimal sized domains where only one $\sqrt{3}\times\sqrt{3}$ unit cell is accommodated inside them.

The sharpness of the $\sqrt{3}\times\sqrt{3}$ spots throughout the transition from α- to β-$\sqrt{3}\times\sqrt{3}$ do not mean large domain size, or long-range order in an ordinary sense. The long-range order here, arises from the fact that the coherence is kept among the small domains that belong to one type of the sublattices of $\sqrt{3}\times\sqrt{3}$ superstructure. For simplicity, Figs. 7(a)–7(c) are composed of two types of domains. Domains of one type are made in a large domain of another type (so-called ''swiss cheese structure''). The diffraction from the latter large sized domain yields sharp $\sqrt{3}\times\sqrt{3}$ spikes. The interference between the waves diffracted from the two types of domains is not completely destructive, because the phase difference between them is $2\pi/3$. If all the three domains of different three sublattices coexist and their total areas are equivalent, intensities of the $\sqrt{3}\times\sqrt{3}$ spikes are canceled out since the waves diffracted from the respective domains interfere destructively. Thus, the existence of the $\sqrt{3}\times\sqrt{3}$ spikes in the LEED pattern indicates that the ratios among the three different types of domains are not equivalent. This discussion is ascertained by the simulation shown in Fig. 7 where the sharp $\sqrt{3}\times\sqrt{3}$ spikes are reproduced by having one type of the $\sqrt{3}\times\sqrt{3}$ domain be absent.

The observed domain-wall proliferation strongly suggests that the creation of the domain walls is energetically favorable, or at least, does not cost significant energy. The zigzagging feature of the domain walls is most possibly attributed to small tension along them: microscopic origin of this will be the small formation energy of the 60° bending points.

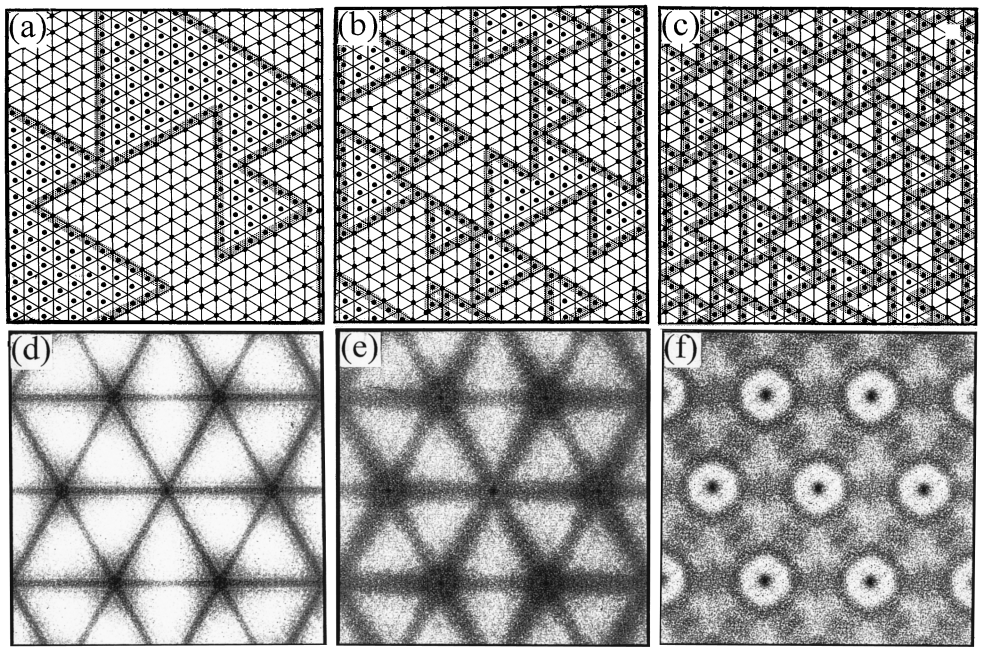

FIG. 7. (a)–(c) Artificially made 2D images imitating some characteristic features in STM images of Fig. 4. The images are composed of two kinds of domains which belong to two different sublattices of the $\sqrt{3}\times\sqrt{3}$ superstructure. Triangular mesh in these figures express the $\sqrt{3}\times\sqrt{3}$ periodicity. Bold gray lines denote the domain boundaries. (c)–(f) Corresponding Fourier-transformed patterns processed from the images in the upper row.

From the STM images, the system appears to try to expand the domain walls as long as possible with a zigzagging feature to lower the free-energy density. The domain walls fold up more tightly as the Au coverage increases,in a way that the domain walls avoid crossing each other. For example, by carefully investigating the STM image in Figs. 4(b), 4(c), the points shown by arrows are not the crossing points; the domain walls just inflect at these points without crossing. Thus, creation of the crossing points is suggested to be energetically unfavorable, and this would produce a nominal short-range repulsion between domain walls. Thus, the agglomeration of the domain walls [white regions in Figs. 3(c)–3(h) and Figs. 4(a)–4(f)] is not observed. Above $\Theta=0.96$, where the density of the domain walls is highest, this short-range repulsion works as a severe constraint for the domain walls to arrange in a short-range order of 6**a** which corresponds to the size of minimal $\sqrt{3}\times\sqrt{3}$ domains [see Fig. 7(c)].

B. Temperature dependence at $\Theta=0.79$: Sweep out of domain walls at high temperatures

It has been known that the fine structures in the $\sqrt{3}\times\sqrt{3}$ patterns disappear at elevated temperatures.[10,22,27] However, up to now, no detailed discussion concerning the behavior of the domain walls and the diffraction patterns at high temperatures has been reported.

Temperature-variable spot profile measurements were performed at $\Theta=0.79$ (Fig. 8). Figure 8(a) shows an identical profile to Fig. 6(a). Shoulders at sharp spikes due to the domain walls are clearly visible at temperatures below 773 K. However, these fine structures become very weak at 773 K, while the sharp $\sqrt{3}\times\sqrt{3}$ spikes persist. At temperatures above 873 K only the sharp spikes are observed with uniformly distributed background. This change strongly suggests extinction of domain walls and growth of large $\sqrt{3}\times\sqrt{3}$ single domains. This behavior is quite unexpected and unusual since the most reported order-disorder phase transitions show ordered phases at low temperatures and disordered phases at high temperatures.[1–8] The present case is quite opposite because it shows a disordered (or a partially ordered) structure at low temperatures and an apparent well-ordered structure at high temperatures.

This perplexing result can be correctly understood by concentrating our attention on the behavior of the domain walls, not on the $\sqrt{3}\times\sqrt{3}$ mesh. Figure 9 shows temperature variable STM pictures for α-$\sqrt{3}\times\sqrt{3}$ structure taken in current imaging mode. Zigzagging domain walls running in [112] directions at RT converts to more roundish ones at 753 K [Fig. 9(b)] and show sluggish fluidity. This feature corresponds to the increase in the meandering entropy of the domain walls which results in the free-energy gain of the system. In this context, the absence of domain walls at 893 K [Fig. 9(c)], should be assigned to the decomposition of domain walls that corresponds to the state of the highest entropy with scattered excess Au atoms. That is, the domain wall ''evaporates'' into its gas phase where the excess Au atoms consisting of the domain walls distribute randomly (in mobile) on the surface or in the subsurface region. This interpretation is not unreal at all since analogous behavior is reported for the Si(111)-5×2-Au surface; movements in par-

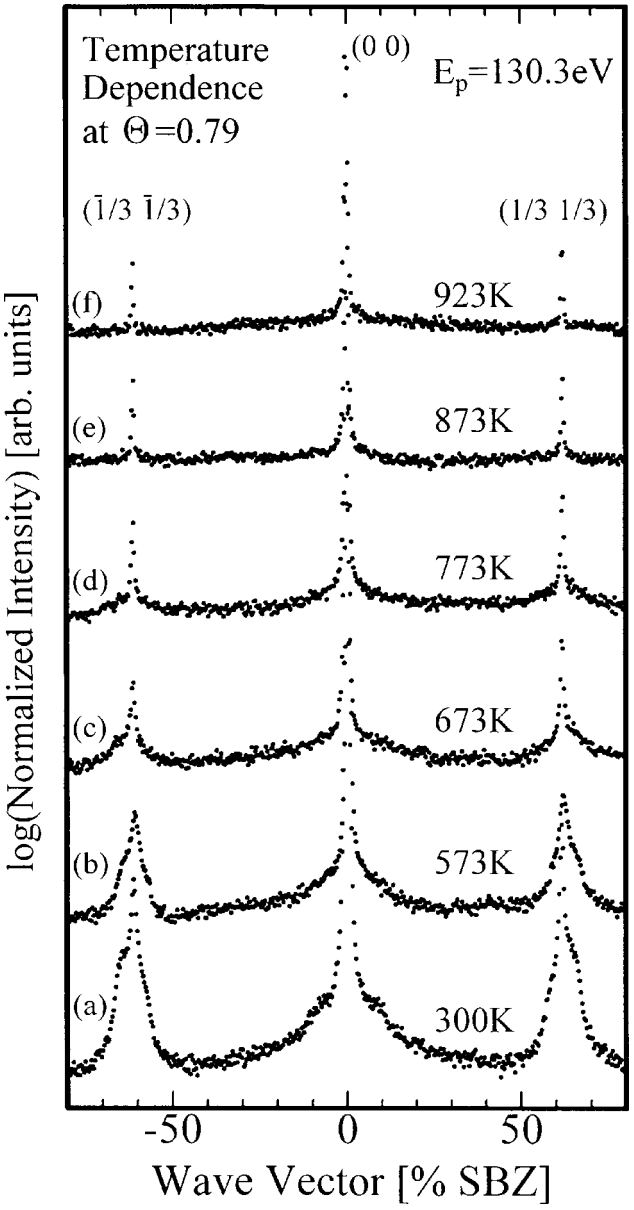

FIG. 8. Temperature dependence of spot profiles in (00)-(11) direction. This sequence corresponds to ② in Fig. 2. Up to 673 K, characteristic fine features of α-$\sqrt{3}\times\sqrt{3}$ pattern persist, but above 773 K, these fine features disappear. Intensities are normalized to that of (00) spikes and are shown in logarithmic scale.

tially ordered arrays of adatoms in STM images become faster with temperature and finally become invisible to become an apparently well-ordered 5×1 phase.[16,28] Other theoretical and experimental reports concerning the domain-wall evaporation are also given in Refs. 29–32. The above discussions are understandable from the viewpoint of free energy; the high-temperature phase [Fig. 9(c)] gets entropy by some random distribution of the excess Au atoms. Thus, the observed transitions might be described adequately as ''domain-wall melting'' [Fig. 9(b)] and the following ''domain-wall evaporation'' [Fig. 9(c)] with the increase of temperature.

It should be noted that the feature of Fig. 9(a) is reproducible after heating around 800 K irrespective of the cooling procedure (e.g., quench cooling or slow cooling; process ② in Fig. 2). This is not the case above $\Theta=0.96$ (β-$\sqrt{3}\times\sqrt{3}$ and 6×6 structures) as we will see in the next subsection.

C. Temperature dependence at $\Theta=1.0$: Transition between metastable β-$\sqrt{3}\times\sqrt{3}$ and stable 6×6

The β-$\sqrt{3}\times\sqrt{3}$ and the 6×6 structures are formed at the same Au coverage above $\Theta=0.96$. The β-$\sqrt{3}\times\sqrt{3}$ is formed by quench cooling after annealing above 640 K, while the 6×6 is formed by mild heating around 600 K followed by slow cooling. This indicates that the β-$\sqrt{3}\times\sqrt{3}$ is just a metastable structure and the 6×6 is a stable true phase.

Figure 10 shows temperature-variable spot profile measurements taken at $\Theta=1.0$. Figure 10(a) shows a profile of the 6×6 phase at RT. The diffraction keeps the 6×6 pattern up to 640 K but it converts to sharp a $\sqrt{3}\times\sqrt{3}$ pattern [Fig. 10(c)] at higher temperatures similar to the case with Figs. 8(e), 8(f). The diffraction converts to that of the β-$\sqrt{3}\times\sqrt{3}$ pattern after sudden stop of the heating current [Fig. 10(d) which is similar to Fig. 6(e)]. This pattern is transformed back to that of Fig. 10(a) by annealing at 600 K followed by slow cooling.

Figure 11 shows STM images (current images) of three different structures prepared by different procedures at $\Theta=1.0$. Since a good topographic image is not obtained at high temperature due to the thermal drift, the images are taken in the current imaging mode with faster scans. Figure 11(b) was taken at 893 K ($\sqrt{3}\times\sqrt{3}$-sharp). Figure 11(a) was taken after quench cooling the sample from 893 K (β-$\sqrt{3}\times\sqrt{3}$). Figure 11(c) was taken after slowly cooling the sample after annealing at 893 K (6×6). In contrast to the clear long-range order with 6×6 periodicity in Fig. 11(c), clear structural features are not recognized in Fig. 11(a) except protrusions with separations around $\sqrt{3}\mathbf{a}$. However, corresponding LEED pattern and the Fourier-transformed pattern of the STM image show clear short-range order with $6\mathbf{a}$ [e.g., rings in β-$\sqrt{3}\times\sqrt{3}$ pattern in Fig. 5(d)]. The high-temperature $\sqrt{3}\times\sqrt{3}$ structure [Fig. 11(b)] shows no domain walls. This structure is expected to be the same structure as Fig. 9(c). A RHEED rocking curve measurement at elevated temperature showed small coverage dependence which is consistent with our discussion.[33] The excess amount of Au coverage will be accommodated in the gas phase on the $\sqrt{3}\times\sqrt{3}$ surface or in the subsurface region.

A schematic figure for illustrating the structure transformation is shown in Fig. 12. Figure 12(a) corresponds to the well ordered $\sqrt{3}\times\sqrt{3}$ structure with evaporated atoms from domain walls, corresponding to Fig. 11(b). If the surface is cooled slowly from Fig. 12(a), the domain walls are efficiently recrystallized to form the long-range ordered 6×6 phase [Fig. 12(c)], corresponding to Fig. 11(c). If the cooling speed is not slow enough, the local structure at the domain-wall liquid phase is frozen and just a metastable β-$\sqrt{3}\times\sqrt{3}$ structure is formed [Fig. 12(b)], corresponding to Fig. 11(c).

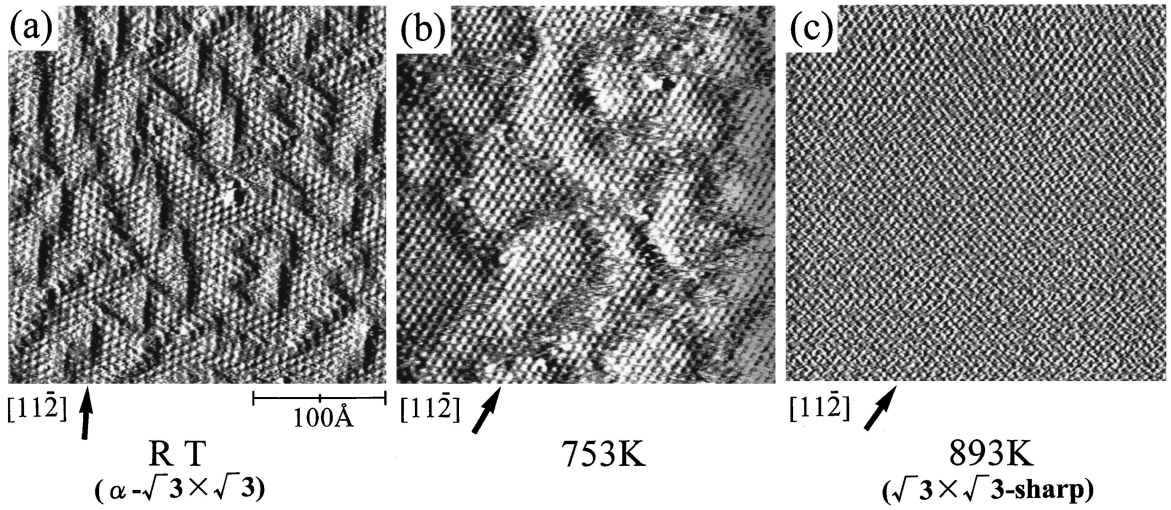

FIG. 9. Temperature-variable STM images at $\Theta=0.79$ (α-$\sqrt{3}\times\sqrt{3}$). The zigzagging domain configuration at RT changes to a roundish one at 753 K. At 893 K, the domain walls are decomposed completely.

In the β-$\sqrt{3}\times\sqrt{3}$ structure, a short-range order of 6**a** is present instead of the lack of long-range order of 6×6. This was confirmed in the same simulation as Fig. 7 that the rings were not reproduced when the long-range order of 6×6 with some defects was assumed in the simulated 2D image. Since the ''lack of long-range order and the presence of short-range order'' is the principal nature which characterizes the amorphous structure, an adequate description of the β-$\sqrt{3}\times\sqrt{3}$ structure will be an amorphouslike (glasslike) structure in the arrangement of domain walls, as sketched in Fig. 12(b). In this context, the 6×6 structure will be described as crystalline structure in the arrangement of domain walls, as depicted in Fig. 12(c). Since the movement of domain walls are expected to be very slow compared to that of single atoms, it is understandable that the transition between the β-$\sqrt{3}\times\sqrt{3}$ and the 6×6 structure behaves like commonly observed glass transitions which normally require mild heating and large mass transport for the formation of a crystal phase.

In contrast to the behavior above $\Theta=0.96$, the recrystallization of the domain walls is not observed at lower coverages where the domain-wall separation is larger (e.g., the α-$\sqrt{3}\times\sqrt{3}$ structure, Fig. 9). This fact, again, strongly suggests that existence of the nominal short-range repulsion between the domain walls mentioned at the end of Sec. III A.

IV. SUMMARY

The phase transitions among the α-$\sqrt{3}\times\sqrt{3}$, β-$\sqrt{3}\times\sqrt{3}$, and 6×6 patterns in electron diffraction have been correlated to the behaviors of domain walls observed by STM. An adequate description of the behavior of the domain walls is summarized in a schematic phase diagram shown in Fig. 2. The density of the domain walls between out-of-phase $\sqrt{3}\times\sqrt{3}$ domains starts to increase from $\Theta=0.76$ with the Au coverage and stops increasing at $\Theta=0.96$ where they are most densely packed. This behavior strongly suggests an energy gain by elongation of the domain walls and short-range repulsion between the domain walls. The sharp $\sqrt{3}\times\sqrt{3}$ superlattice spots persistent during this structural change have been correlated to the unequal area distribution among the

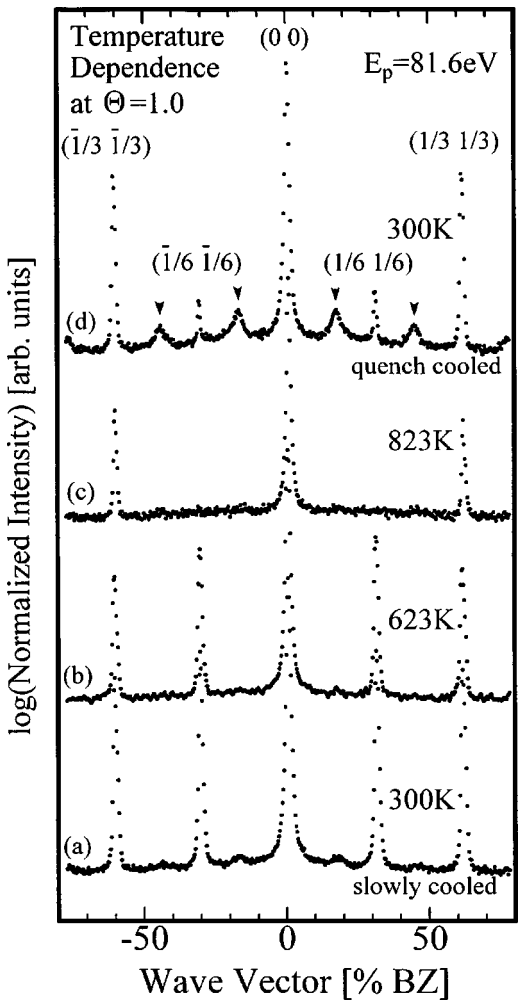

FIG. 10. Spot profiles in the (00)-(11) direction at $\Theta=1.0$ taken as a function of temperature. This sequence corresponds to ③ in Fig. 2. The 6×6 pattern was formed by annealing at 600 K and then slowly cooled (a). Up to 640 K, 6×6 spikes persist, but above 640 K, only the $\sqrt{3}\times\sqrt{3}$ spikes survive (b) and (c). After heating at 823 K and then quench cooled, features correspond to rings in β-$\sqrt{3}\times\sqrt{3}$ pattern [arrowheads in (d)] appear. Intensities are normalized to (00) spikes and are shown in logarithmic scale.

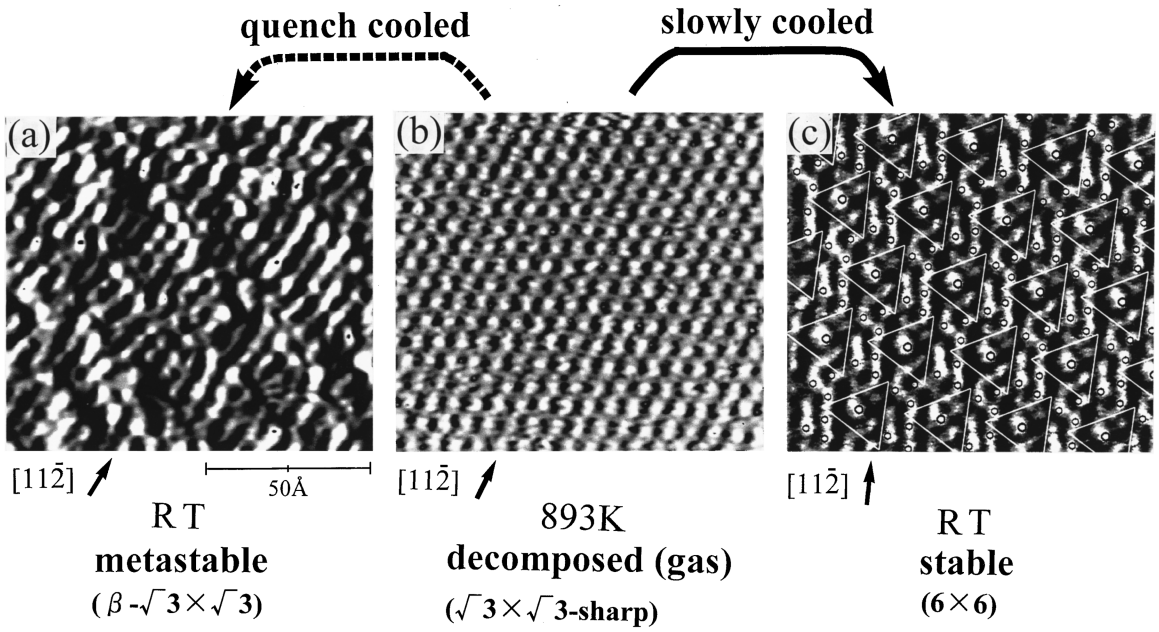

FIG. 11. STM images of three different structures formed at $\Theta = 1.0$. (a) (β-$\sqrt{3}\times\sqrt{3}$) structure prepared by quench cooling after heating at 893 K. (b) $\sqrt{3}\times\sqrt{3}$ structure at 893 K. (c) 6×6 structure prepared by slow cooling after heating at 893 K. Triangles and open circles correspond to the schematic model as shown in Fig. 12(c).

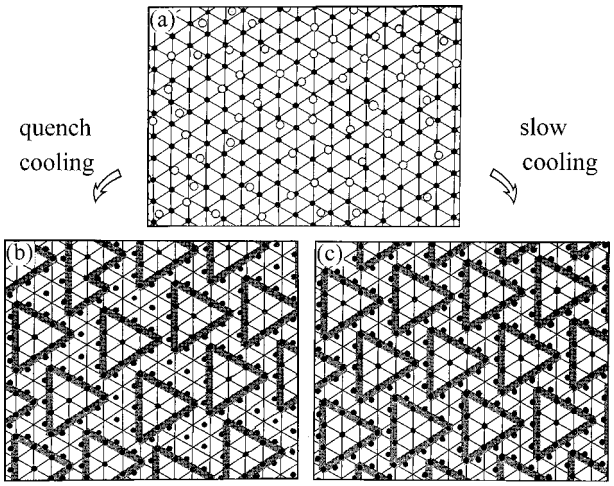

FIG. 12. Schematic illustration describing the three different structures above $\Theta = 0.96$. (a) Domain walls are evaporated to form a gas phase at high temperature. (b) Minimum-sized domains are densely random packed to form a short-range order with the nearest-neighbor distance around 6**a** (domain-wall glass). (c) Minimum-sized domains are arranged in a closed-packed structure to form a long-range order of 6×6 (domain-wall crystal). The triangular lattice shows the $\sqrt{3}\times\sqrt{3}$ periodicity. Open circles in (a) express the atoms kicked out from the domain walls. Filled circles represent the $\sqrt{3}\times\sqrt{3}$ periodicity with different phases of sublattices; they do not represent the real atoms. Gray lines express the domain walls between the out-of-phase $\sqrt{3}\times\sqrt{3}$ domains.

three domains of different three sublattices of $\sqrt{3}\times\sqrt{3}$ superstructure.

The domain walls are transformed from zigzagging ones running in [112] directions to disordered roundish ones and are decomposed completely as the temperature increases. This change should be associated with the entropy gain which contributes to the decrease in free energy.

Quench cooling or slow cooling do not affect the domain structure at coverages lower than $\Theta = 0.96$ (mainly at α-$\sqrt{3}\times\sqrt{3}$, indicated by ② in Fig. 2), since the effect of short-range repulsion among domain walls is minute due to their large separation. On the other hand, the difference in cooling procedures makes large difference in the structure above $\Theta = 0.96$ where the domain-wall density is maximum (indicated by ③ in Fig. 2). Slow cooling yields a stable long-range ordered 6×6 phase while quench cooling yields a metastable short-range ordered β-$\sqrt{3}\times\sqrt{3}$ structure. Adequate names which describe the character of these two structures will be ''domain-wall crystal'' and ''domain-wall glass,'' respectively.

ACKNOWLEDGMENTS

This work has been supported in part by Grants-in-Aid from the Ministry of Education, Science, Culture, and Sports of Japan, especially through the New Frontier Program Grants-in-Aid for Scientific Research (Nos. 08NP1201 and 09NP1201) and the International Scientific Research Program (No. 07044133), conducted by Professor K. Yagi of Tokyo Institute of Technology. This work has also been supported by the Japan Securities Scholarship Foundation and Nippon Sheet Glass Foundation for Materials Science and Engineering.

*Author to whom correspondence should be addressed. Electronic address: nagao@phys.s.u-tokyo.ac.jp
†Present address: Faculty of Engineering, Utsunomiya University, 2573 Ishii-cho, Utsunomiya, Tochigi 321, Japan.

[1] H. Pfnür and P. Piercy, Phys. Rev. B **40**, 2515 (1989).
[2] M. Sokolowsky and H. Pfnür, Phys. Rev. B **49**, 7716 (1994).
[3] L. Schwenger, K. Budde, C. Voges, and H. Pfnür, Phys. Rev. Lett. **73**, 296 (1994).
[4] C. Voges, K. Budde, and H. Pfnür, Surf. Sci. **338**, L839 (1995).
[5] S. Hasegawa, Y. Nagai, T. Oonishi, and S. Ino, Phys. Rev. B **47**, 9903 (1993).
[6] S. Hasegawa, Y. Nagai, T. Oonishi, N. Kobayashi, T. Miyake, S. Murakami, Y. Ishii, D. Hanawa, and S. Ino, Phase Transit. **53**, 87 (1994).
[7] Y. Nakajima, C. Voges, T. Nagao, G. Kloss, H. Pfnür, and S. Hasegawa, Phys. Rev. B **55**, 8129 (1997).
[8] J. S. Hong, H. W. Kim, H. J. Kim, and J. W. Chung, Phys. Rev. B **55**, 7047 (1996).
[9] G. LeLay, Surf. Sci. **132**, 169 (1983).
[10] S. Ino, in *Reflection High Energy Electron Diffraction and Reflection Electron Imaging of Surfaces*, edited by P. K. Larsen and P. J. Dobson (Plenum, New York, 1988); S. Ino, J. Phys. Soc. Jpn. **37**, 82 (1982) (in Japanese).
[11] E. Bauer, Surf. Sci. Lett. **250**, L379 (1991).
[12] H. Daimon, C. Chung, Y. Watanabe, and S. Ino, Surf. Sci. **235**, 142 (1990).
[13] S. Takahashi, Y. Tanishiro, and K. Takayanagi, Surf. Sci. **242**, 73 (1991).
[14] K. Higashiyama, S. Kono, and T. Sagawa, Jpn. J. Appl. Phys., Part 2 **25**, L117 (1986).
[15] A. A. Baski, J. Nogami, and C. F. Quate, Phys. Rev. B **41**, 10 247 (1990).
[16] T. Hasegawa, S. Hosaka, and S. Hosoki, Jpn. J. Appl. Phys., Part 2 **31**, L1492 (1992).
[17] J. D. O'Mahony *et al.*, Surf. Sci. Lett. **277**, L57 (1992).
[18] J. Nogami, A. A. Baski, and C. F. Quate, Phys. Rev. Lett. **65**, 1611 (1990).
[19] T. Takami, D. Fukushi, T. Nakayama, M. Uda, and M. Aono, Jpn. J. Appl. Phys., Part 1 **33**, 3688 (1994).
[20] J. Falta *et al.*, Surf. Sci. **330**, L673 (1995).
[21] R. Plass and L. D. Marks, Surf. Sci. **342**, 233 (1995).
[22] K. Tsuno, Ph.D. thesis, University of Tokyo, 1990.
[23] K. Oura, M. Katayma, F. Shoji, and T. Hanawa, Phys. Rev. Lett. **55**, 1486 (1985).
[24] J. H. Huang and R. S. Williams, Phys. Rev. B **38**, 4022 (1988).
[25] M. Chester and T. Gustafsson, Surf. Sci. **256**, 135 (1991).
[26] T. Nagao, C. Voges, H. Pfnür, M. Henzler, S. Ino, and S. Hasegawa, Appl. Surf. Sci. (to be published).
[27] S. Hasegawa and S. Ino, Int. J. Mod. Phys. B **7**, 3817 (1993).
[28] T. Hasegawa, S. Hosaka, and S. Hosoki (unpublished).
[29] I. F. Lyuksyutov, H. Pfnür, and H.-U. Everts, Europhys. Lett. **33**, 673 (1996).
[30] M. Stolzenberg, I. L. Lyuksyutov, and E. Bauer, Phys. Rev. B **42**, 10 714 (1990).
[31] E. V. Klimenko, E. M. Litvinova, I. F. Lyuksyutov, A. G. Naumovets, and I. N. Zasimovich, Surf. Sci. **271**, 244 (1992).
[32] M. Stolzenberg, I. L. Lyuksyutov, and E. Bauer, Phys. Rev. B **48**, 2675 (1993).
[33] E. A. Khramtsova and A. Ichimiya (private communication).